Alexandria Engineering Journal (2020) 59, 1869–1879

HOSTED BY

Alexandria University

Alexandria Engineering Journal

www.elsevier.com/locate/aej
www.sciencedirect.com

Flow and heat transfer past a permeable power-law deformable plate with orthogonal shear in a hybrid nanofluid

Najiyah Safwa Khashi'ie [a,b,*], Norihan Md Arifin [a,c], Ioan Pop [d], Roslinda Nazar [e], Ezad Hafidz Hafidzuddin [f], Nadihah Wahi [c]

[a] *Institute for Mathematical Research, Universiti Putra Malaysia, 43400 UPM Serdang, Selangor, Malaysia*
[b] *Fakulti Teknologi Kejuruteraan Mekanikal dan Pembuatan, Universiti Teknikal Malaysia Melaka, Hang Tuah Jaya, 76100 Durian Tunggal, Melaka, Malaysia*
[c] *Department of Mathematics, Faculty of Science, Universiti Putra Malaysia, 43400 UPM Serdang, Selangor, Malaysia*
[d] *Department of Mathematics, Babeş-Bolyai University, R-400084 Cluj-Napoca, Romania*
[e] *School of Mathematical Sciences, Faculty of Science and Technology, Universiti Kebangsaan Malaysia, 43600 UKM Bangi, Selangor, Malaysia*
[f] *Centre of Foundation Studies for Agricultural Science, Universiti Putra Malaysia, 43400 UPM Serdang, Selangor, Malaysia*

Received 4 February 2020; revised 1 May 2020; accepted 21 May 2020
Available online 4 June 2020

KEYWORDS

Stretching/shrinking surface;
Three dimensional;
Hybrid nanofluid;
Heat transfer;
Dual solutions

Abstract This study concerns the three-dimensional hybrid nanofluid flow and heat transfer due to a deformable (stretching/shrinking) plate with power-law velocity and orthogonal surface shear. The flow due to the shrinking sheet is maintained with the imposition of wall mass suction. The effect of adding Cu and Al_2O_3 nanoparticles are represented by a homogeneous mixture model with the modified thermophysical properties. Two types of thermophysical properties for hybrid nanofluids are discussed and compared in this interesting work. The three-dimensional model is then, reduced into a relevant set of ordinary differential equations using similarity transformation. The results are generated using the bvp4c solver and presented in the tables and graphs. Duality of solutions are observed in both stretching and shrinking regions, however, only the first solution is proved to be stable and realistic. Surprisingly, the heat transfer rate augments when the power law velocity is used. The hybrid nanofluid with an upsurge of copper volume fraction also reduces the rate of heat transfer.

© 2020 The Authors. Published by Elsevier B.V. on behalf of Faculty of Engineering, Alexandria University. This is an open access article under the CC BY-NC-ND license (http://creativecommons.org/licenses/by-nc-nd/4.0/).

1. Introduction

Flow induced by a stretching sheet has been topic of interest for most researchers in the area of fluid dynamics due to its applicability in many industrial and engineering sectors. Crane

* Corresponding author at: Fakulti Teknologi Kejuruteraan Mekanikal dan Pembuatan, Universiti Teknikal Malaysia Melaka, Hang Tuah Jaya, 76100 Durian Tunggal, Melaka, Malaysia.
E-mail address: najiyah@utem.edu.my (N.S. Khashi'ie).
Peer review under responsibility of Faculty of Engineering, Alexandria University.

https://doi.org/10.1016/j.aej.2020.05.029
1110-0168 © 2020 The Authors. Published by Elsevier B.V. on behalf of Faculty of Engineering, Alexandria University.
This is an open access article under the CC BY-NC-ND license (http://creativecommons.org/licenses/by-nc-nd/4.0/).

[1] focused on stretching flow with linear velocity and obtained the suited exact solution of the Navier-Stokes equations. Banks [2] reported the boundary layer solutions of flow due to a power-law stretching surface ($u = ax^n$) with zero pressure gradient. Later, Weidman [3] proposed three generalizations of Banks' power law stretching for three-dimensional flow; first extension by including an arbitrary transverse shear $\alpha(y)$ with $v = 0$ so that $u = ax^n\alpha(y)$, second extension by letting $u = a[x + \alpha(y)]^n$ with $v = 0$ and the last generalization by considering an orthogonal power-law shearing motion so that $u = ax^n$ and $v = bx^n$. Previously in 2013, Weidman [4] showed that a transpiration (suction) effect was necessary to induce the uniform shear flow while the combination of linear stretching and shear flows could exist without the transpiration. Weidman [5] investigated orthogonal linear stretching and shearing motions due to an impermeable surface while Weidman et al. [6] analyzed the rotating flow past an impermeable surface with biaxial linear stretching and shearing motions. Goldstein [7] discussed the behaviour of shrinking sheet which produced a backward or reverse flow. Different with stretching flow, the shrinking flow was shown to discontinue without the transpiration (suction) effect as discovered by Miklavčič and Wang [8]. They showed that no solution was attained when suction $s < 2$ (in their notation), unique at $s = 2$ and dual solutions when $s > 2$. Fang [9] investigated the boundary layer flow induced by a shrinking sheet with power-law or nonlinear velocity. Fang [9] found the existence of multiple solutions within the certain range of suction and power index controlling parameters. However, both literatures [8,9] did not report on the flow stability.

A new generation of fluid with good thermal performance is beneficial to fulfil the industrial or technological needs. Hybrid nanofluid combines a base fluid (i.e. water, ethylene glycol, mixture of ethylene glycol and water) with two different types of nanoparticles (i.e. metal oxides, metals, carbon materials). According to Suresh et al. [10], the combination of least and suitable amounts of copper nanoparticles into the alumina matrix could maintain the stability of the resulting hybrid nanofluid. Alumina nanoparticle has a good chemical inaction and stability although the thermal conductivity is lower than the copper nanoparticle. Mansoury et al. [11] analyzed the heat transfer performance of parallel flow heat exchangers using alumina-water nanofluid. They found that the double-pipe heat exchanger had the maximum heat transfer enhancement than the plate heat exchanger and two shell-and-tube heat exchangers. The natural convection heat transfer of CuO-water nanofluid in a U-shaped enclosure equipped by a baffle was numerically investigated by Ma et al. [12]. They showed that an increase in nanoparticle volume fraction led to the increment of average Nusselt number. Further, the reviews on the applications, preparation and thermophysical properties of the regular and hybrid nanofluids have been conducted by these researchers (see Jana et al. [13], Sarkar et al. [14], Sidik et al. [15], Akilu et al. [16], Babu et al. [17], Sundar et al. [18], Leong et al. [19], Huminic and Huminic [20] and Sajid and Ali [21]). Further, the research on hybrid nanofluids consisting of nano-encapsulated phase change materials also attract many researchers (see Ghalambaz et al. [22–24] and Hajjar et al. [25]). The heat transfer process related to a cavity also has been subject of interest due to its numerous engineering operations such as in heat exchangers, HVAC (heating, ventilation and air conditioning) and building insulation. Chamkha et al. [26] performed the numerical simulation for hybrid Cu-Al_2O_3/water nanofluid flow and heat transfer from a cavity. Ghalambaz et al. [27] analyzed Ag–MgO hybrid nanofluid flow and heat transfer inside a porous square cavity using the local thermal non-equilibrium (LTNE) model. They found that the usage of hybrid nanoparticles reduced the flow strength and heat transfer rate. The thermogravitational convection of hybrid Al_2O_3-SiO_2/water nanofluid in a porous chamber was scrutinized by Sheremet et al. [28].

Devi and Devi [29,30] modified the thermophysical correlations for hybrid nanofluid and used them along with the single phase nanofluid mathematical model by Tiwari and Das [31] to stretching flow problems. The thermophysical properties had an excellent agreement with the existing experimental data by Suresh et al. [10]. This single phase model by Tiwari and Das [31] was frequently adopted because it featured the effect of governing nanoparticle volume fraction in heat transfer rate. However, this model was restricted to the spherical-shaped nanoparticle only [32]. For nanofluid particularly using Cu-Al_2O_3 hybrid nanoparticles, Waini et al. [33,34] reported the existence of dual solutions using nonlinear and linear stretching/shrinking plate velocity, respectively. Meanwhile, Waini et al. [35] studied the transpiration effects on hybrid nanofluid flow induced by power-law stretching/shrinking sheet with uniform shear flow. They also reported that the heat transfer rate enhanced for both stretching and shrinking cases with the accretion of copper volume fraction. However, Khashi'ie et al. [36] revealed that the enhancement of copper volume fractions could reduce the heat transfer rate for the shrinking case as a result of higher suction, which is in accordance with findings by Waini et al. [33,34]. Lund et al. [37] examined hybrid Cu-Al_2O_3/water nanofluid flow over a nonlinear shrinking sheet with the presence of viscous dissipation. They perceived two solutions and concluded that the increasing values of copper or alumina nanoparticles diminished the heat transfer rate. Other numerical works on hybrid nanofluid flow due to stretching and shrinking surfaces were also considered by Dinarvand et al. [38–40], Aly and Pop [41], Farooq et al. [42] and Khashi'ie et al. [43,44].

Therefore, inspired by the above-mentioned literatures, the present work focuses on the hybrid nanofluid flow and heat transfer induced by a power-law (nonlinear) stretching/shrinking plate with orthogonal surface shear as studied by Weidman [3]. The novelty of the present work is by including the energy equation (heat transfer observation) and utilizing the homogeneous mixture model with modified thermophysical properties as studied by Devi and Devi [29,30] to represent the hybrid Cu-Al_2O_3/water nanofluid which is not considered by Weidman [3] and other researchers. In the present investigation, 10% (0.1) alumina volumetric concentration is fixed whereas the effect of varied copper volumetric concentration and other parameters are investigated. The availability of two solutions are observed; hence the transpiration effect is also within the scope of study. The authors believe that no similar work has been considered or published by other researchers. The finding will benefit other researchers in predicting the behaviour of nanofluids (traditional and hybrid) flow and relevant parameters for heat transfer performance.

2. Mathematical formulation

The present work accentuates the extension of Banks [2] problem reported by Weidman [3] using Cu-Al_2O_3/water hybrid nanofluid. Consider the three-dimensional flow utilizing the Cartesian coordinate (x, y, z) where x and y are the streamwise and spanwise directions, respectively while z is normal to the plate as shown in Fig. 1. The corresponding velocities (u, v, w) are assumed align with the Cartesian coordinate (x, y, z). One of the generalization of Banks' power-law stretching by including an orthogonal power-law shearing motion of the sheet/plate (see Weidman [3]). The plate motion is $u_w = ax^n$ and $v_w = bx^n$. Further, it is assumed that the wall temperature (T_w) is constant and higher than the ambient temperature (T_∞) because the heat transfer process occurs from the plate to the ambient fluid.

The governing boundary layer equations are constituted by the continuity, streamwise and spanwise momentum equations together with the energy equation (see Weidman [3], Devi and Devi [29,30])

$$\frac{\partial u}{\partial x}+\frac{\partial v}{\partial y}+\frac{\partial w}{\partial z}=0, \tag{1}$$

$$u\frac{\partial u}{\partial x}+v\frac{\partial u}{\partial y}+w\frac{\partial u}{\partial z}=\nu_{hnf}\frac{\partial^2 u}{\partial z^2}, \tag{2}$$

$$u\frac{\partial v}{\partial x}+v\frac{\partial v}{\partial y}+w\frac{\partial v}{\partial z}=\nu_{hnf}\frac{\partial^2 v}{\partial z^2}, \tag{3}$$

$$u\frac{\partial T}{\partial x}+v\frac{\partial T}{\partial y}+w\frac{\partial T}{\partial z}=\alpha_{hnf}\frac{\partial^2 T}{\partial z^2}, \tag{4}$$

while the boundary conditions are

$$u(x,y,0)=\lambda u_w,\ v(x,y,0)=\lambda v_w,\\ w(x,y,0)=w_0,\ T(x,y,0)=T_w, \tag{5}$$

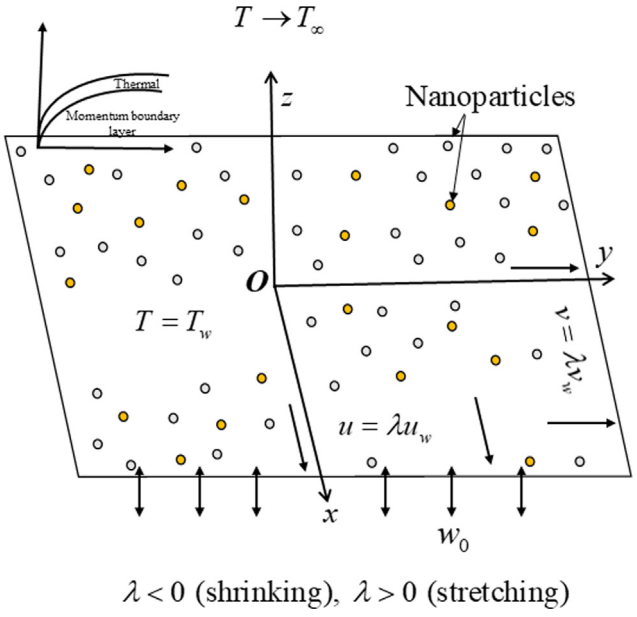

Fig. 1 The physical model and coordinate system.

$$u(x,y,z)\to u_w,\ v(x,y,z)\to v_w,\ T(x,y,z)\to T_\infty \text{ as } z\to\infty \tag{6}$$

where T is the hybrid nanofluid temperature, $\nu_{hnf}=\mu_{hnf}/\rho_{hnf}$ denotes the kinematic viscosity of the hybrid nanofluid, $\alpha_{hnf}=k_{hnf}/(\rho C_p)_{hnf}$ stands for the thermal diffusivity of the hybrid nanofluid while k_{hnf}, $(\rho C_p)_{hnf}$, μ_{hnf} and ρ_{hnf} represent the thermal conductivity, heat capacity, dynamic viscosity and density of the hybrid nanofluid, correspondingly. In addition, λ is the stretching/shrinking parameter (constant) with $\lambda > 0$ symbolizes the stretching sheet, $\lambda < 0$ for the shrinking sheet and $\lambda = 0$ refers to a static plate.

2.1. Thermophysical properties

The physical properties between nanofluid and hybrid nanofluid are elucidated in Table 1 where s, f, nf and hnf represent nanoparticles, regular fluid, mono and hybrid nanofluids, respectively. ϕ is the nanoparticles volume fraction; ϕ_1 stands for first nanoparticle volume fraction while ϕ_2 for second nanoparticle volume fraction. In the present work, we adopt the thermophysical properties for Cu-Al_2O_3/water hybrid nanofluid proposed by Devi and Devi [29,30] which has been validated with the experimental work of Suresh et al. [10]. Devi and Devi [29] fixed the volumetric concentration of alumina as $\phi_1 = 0.1$ (10%) while varied the volumetric concentration of copper nanoparticles. It is assumed that the alumina nanoparticles were dispersed into the pure water to form Al-water nanofluid. Copper nanoparticles were then added to create the Cu-Al_2O_3/water hybrid nanofluid. However, a few of presumptions are also examined for the physical model:

- The nanofluid is assumed to be stable; hence the effect of nanoparticles aggregation and sedimentation is omitted.
- The nanoparticles are uniform with a spherical shape.
- The base fluid and nanoparticles are maintained in a thermal equilibrium state.

The thermo-physical properties of the water, alumina and copper nanoparticles as envisaged by Khanafer et al. [45] and Oztop and Abu-Nada [46] are exemplified in Table 2.

It is worth mentioning that there is also another practical correlations of hybrid nanofluids as discussed by Babu et al. [17], Takabi and Salehi [47], Ghalambaz et al. [48] and Tayebi and Chamkha [49]. In the model, the volume fraction of hybrid nanoparticles is represented by the addition of both nanoparticles such that $\phi_{hnf}=\phi_1+\phi_2$ while the density, heat capacity, dynamic viscosity and thermal conductivity are summarized in Table 3.

2.2. Similarity transformation

According to Weidman [3], the continuity Eq. (1) is fulfilled if the similarity variables for the velocities are

$$u=ax^n f'(\eta),\ v=bx^n g'(\eta),\ w=-\frac{\sqrt{a\nu_f}}{\mu}\left[nx^{n-1}f(\eta)+x^n\frac{\mu_x}{\mu}(\eta f'(\eta)-f(\eta))\right],\\ \eta=\sqrt{\frac{a}{\nu_f}}\mu(x)z, \tag{7}$$

where $\mu=\mu(x)$ and $\mu_x = d\mu/dx$. Using (7), the $x-$ and $y-$ momentum equations (see Eqs. (2) and (3)) are

Table 1 The physical properties of nanofluid and hybrid nanofluid (see Devi and Devi [29,30]).

Properties	Nanofluid	Hybrid nanofluid
Density (ρ)	$\rho_{nf} = (1-\phi)\rho_f + \phi\rho_s$	$\rho_{hnf} = (1-\phi_2)\left[(1-\phi_1)\rho_f + \phi_1\rho_{s1}\right] + \phi_2\rho_{s2}$
Heat Capacity(ρC_p)	$(\rho C_p)_{nf} = (1-\phi)(\rho C_p)_f + \phi(\rho C_p)_s$	$(\rho C_p)_{hnf} = (1-\phi_2)\left[(1-\phi_1)(\rho C_p)_f + \phi_1(\rho C_p)_{s1}\right] + \phi_2(\rho C_p)_{s2}$
Dynamic Viscocity(μ)	$\frac{\mu_{nf}}{\mu_f} = \frac{1}{(1-\phi)^{2.5}}$	$\frac{\mu_{hnf}}{\mu_f} = \frac{1}{(1-\phi_1)^{2.5}(1-\phi_2)^{2.5}}$
Thermal Conductivity (k)	$\frac{k_{nf}}{k_f} = \left[\frac{k_s+2k_f-2\phi(k_f-k_s)}{k_s+2k_f+\phi(k_f-k_s)}\right]$	$\frac{k_{hnf}}{k_{bf}} = \left[\frac{k_{s2}+2k_{bf}-2\phi_2(k_{bf}-k_{s2})}{k_{s2}+2k_{bf}+\phi_2(k_{bf}-k_{s2})}\right]$ where $\frac{k_{bf}}{k_f} = \left[\frac{k_{s1}+2k_f-2\phi_1(k_f-k_{s1})}{k_{s1}+2k_f+\phi_1(k_f-k_{s1})}\right]$

Table 2 Thermo-physical properties (see Khanafer et al. [45] and Oztop and Abu-Nada [46]).

Physical properties	Water	Al_2O_3	Cu
ρ(kg/m^3)	997.1	3970	8933
C_p(J/kg K)	4179	765	385
k(W/mK)	0.6130	40	400

$$\left(\frac{\mu_{hnf}/\mu_f}{\rho_{hnf}/\rho_f}\right)\mu^2 f''' + \left(nx^{n-1} - \frac{\mu_x}{\mu}x^n\right)ff'' - nx^{n-1}f'^2 = 0 \tag{8}$$

$$\left(\frac{\mu_{hnf}/\mu_f}{\rho_{hnf}/\rho_f}\right)\mu^2 g''' + \left(nx^{n-1} - \frac{\mu_x}{\mu}x^n\right)fg'' - nx^{n-1}f'g' = 0 \tag{9}$$

Following Weidman [3], to possess a similarity equation, the following term was adopted

$$\frac{\mu_x}{\mu} = \frac{Kn}{x} \tag{10}$$

and using integration by parts

$$\mu(x) = Cx^{Kn} \tag{11}$$

such that K and C are constants. Apply Eqs. (10) and (11) into the momentum equations in (8) and (9) so that

$$\left(\frac{\mu_{hnf}/\mu_f}{\rho_{hnf}/\rho_f}\right)f''' + \left(\frac{nx^{n-1} - Knx^{n-1}}{C^2x^{2Kn}}\right)ff'' - \frac{nx^{n-1}}{C^2x^{2Kn}}f'^2 = 0 \tag{12}$$

$$\left(\frac{\mu_{hnf}/\mu_f}{\rho_{hnf}/\rho_f}\right)g''' + \left(\frac{nx^{n-1} - Knx^{n-1}}{C^2x^{2Kn}}\right)fg'' - \frac{nx^{n-1}}{C^2x^{2Kn}}f'g' = 0 \tag{13}$$

Hence, by letting the coefficients of ff'' and fg'' equal to 1,

$$K = \frac{n-1}{2n},\ C = \sqrt{\frac{n+1}{2}} \tag{14}$$

and Eqs. (12) and (13) are simplified into

$$\left(\frac{\mu_{hnf}/\mu_f}{\rho_{hnf}/\rho_f}\right)f''' + ff'' - \frac{2n}{n+1}f'^2 = 0 \tag{15}$$

$$\left(\frac{\mu_{hnf}/\mu_f}{\rho_{hnf}/\rho_f}\right)g''' + fg'' - \frac{2n}{n+1}f'g' = 0 \tag{16}$$

Using (7), (10), (11) and (14), the same procedure is conducted to transform the energy Eq. (4) with $\theta(\eta) = \frac{T-T_\infty}{T_w-T_\infty}$, so that, we get

$$\frac{1}{\Pr}\frac{k_{hnf}/k_f}{(\rho C_p)_{hnf}/(\rho C_p)_f}\theta'' + f\theta' = 0 \tag{17}$$

In addition, the mass flux parameter is given by

$$w_0 = -\frac{\sqrt{av_f}}{\mu(x)}\left(\frac{n+1}{2}\right)x^{n-1}S \tag{18}$$

and the transformed boundary conditions are

$$f(0) = S,\ g(0) = 0,\ f'(0) = g'(0) = \lambda,\ \theta(0) = 1,\ f'(\eta) \to 0,\ g'(\eta) \to 0,\ \theta(\eta) \to 0,\ \text{as } \eta \to \infty \tag{19}$$

Table 3 The thermophysical correlations of hybrid nanofluids (see Babu et al. [17], Takabi and Salehi [47], Ghalambaz et al. [48] and Tayebi and Chamkha [49]).

Properties	Hybrid Nanofluid
Density (ρ)	$\rho_{hnf} = (1-\phi_{hnf})\rho_f + \phi_1\rho_{s1} + \phi_2\rho_{s2}$
HeatCapacity(ρC_p)	$(\rho C_p)_{hnf} = (1-\phi_{hnf})(\rho C_p)_f + \phi_1(\rho C_p)_{s1} + \phi_2(\rho C_p)_{s2}$
Dynamic Viscocity(μ)	$\frac{\mu_{hnf}}{\mu_f} = \frac{1}{(1-\phi_{hnf})^{2.5}}$
Thermal Conductivity(k)	$\frac{k_{hnf}}{k_f} = \left[\frac{\left(\frac{\phi_1k_1+\phi_2k_2}{\phi_{hnf}}\right)+2k_f+2(\phi_1k_1+\phi_2k_2)-2\phi_{hnf}k_f}{\left(\frac{\phi_1k_1+\phi_2k_2}{\phi_{hnf}}\right)+2k_f-(\phi_1k_1+\phi_2k_2)+\phi_{hnf}k_f}\right]$

where $\mathrm{Pr} = \nu_f/\alpha_f = (C_p\mu)_f/k_f$ is the Prandtl number and S is the mass flux parameter (constant) for permeable surface with $S > 0$ for suction and $S < 0$ for injection.

We point out that the present model is reduced to Weidman [3] (see 3rd extension of Bank's problem) if $\phi_1 = \phi_2 = 0$ (viscous fluid), $S = 0$ (impermeable flat plate) and $\lambda = 1$ (stretching sheet) are considered. However, Weidman [3] omitted the energy equation, hence no heat transfer analysis was presented. Further, Eqs. (15) and (19) also can be reduced to Miklavčič and Wang [8] (linear shrinking) and Fang [9] (nonlinear shrinking) when viscous fluid and permeable flat plate are examined. Like Weidman [3], Miklavčič and Wang [8] and Fang [9] also did not consider the energy equation.

The reduced skin friction coefficients C_{fx} and C_{fy} along the x and y axes and the local Nusselt number Nu_x, are defined as

$$C_{fx} = \frac{\tau_{wx}}{\rho_f u_w^2},\ C_{fy} = \frac{\tau_{wy}}{\rho_f v_w^2},\ Nu_x = \frac{xq_w}{k_f(T_f - T_\infty)}, \tag{20}$$

where τ_{wx} and τ_{wy} are the shear stresses in $x-$ and $y-$ directions while q_w is the surface heat flux

$$\tau_{wx} = \mu_{hnf}\left(\frac{\partial u}{\partial z}\right)_{z=0},\ \tau_{wy} = \mu_{hnf}\left(\frac{\partial v}{\partial z}\right)_{z=0},\ q_w = -k_{hnf}\left(\frac{\partial T}{\partial z}\right)_{z=0}. \tag{21}$$

Using (7), (20) and (21), we obtain

$$\begin{aligned} {Re_x}^{1/2}C_{fx} &= \sqrt{\frac{n+1}{2}}\frac{\mu_{hnf}}{\mu_f}f''(0),\\ {Re_y}^{1/2}C_{fy} &= \sqrt{\frac{n+1}{2}}\frac{\mu_{hnf}}{\mu_f}g''(0),\\ {Re_x}^{-1/2}Nu_x &= -\sqrt{\frac{n+1}{2}}\frac{k_{hnf}}{k_f}\theta'(0), \end{aligned} \tag{22}$$

where $Re_x = u_w(x)x/\nu_f$ and $Re_y = v_w(y)y/\nu_f$ are the local Reynolds number.

3. Temporal stability

The temporal stability analysis is necessary to detect the real (physical) solution if dual or multiple solutions exist. However, Weidman [50] proved that there are two physical solutions available from the multiple solutions. Hence, it is inappropriate to declare the first solution is always stable without validating through the stability analysis. It is worth to mention that the first or upper branch solution refers to the first solution which satisfies the boundary condition. The stability formulation is briefly discussed by Khashi'ie et al. [51,52] for nanofluid and Waini et al. [33–35], Khashi'ie et al. [36,43,44] and Lund et al. [37] for hybrid nanofluid. The flow stability is formulated by considering a time variable $\tau = a\mu^2 t$ into a new set of unsteady (with time) governing equations as suggested by Merkin [53].

$$\frac{\partial u}{\partial t} + u\frac{\partial u}{\partial x} + v\frac{\partial u}{\partial y} + w\frac{\partial u}{\partial z} = \nu_{hnf}\frac{\partial^2 u}{\partial z^2}, \tag{23}$$

$$\frac{\partial v}{\partial t} + u\frac{\partial v}{\partial x} + v\frac{\partial v}{\partial y} + w\frac{\partial v}{\partial z} = \nu_{hnf}\frac{\partial^2 v}{\partial z^2}, \tag{24}$$

$$\frac{\partial T}{\partial t} + u\frac{\partial T}{\partial x} + v\frac{\partial T}{\partial y} + w\frac{\partial T}{\partial z} = \alpha_{hnf}\frac{\partial^2 T}{\partial z^2}, \tag{25}$$

The new simplified similarity transformation is

$$\begin{aligned} &u = ax^n\tfrac{\partial f(\eta,\tau)}{\partial \eta},\ v = bx^n\tfrac{\partial g(\eta,\tau)}{\partial \eta},\ \eta = \sqrt{\tfrac{a}{\nu_f}}\sqrt{\tfrac{n+1}{2}}x^{\frac{n-1}{2}}z,\ \tau = a\left(\tfrac{n+1}{2}\right)x^{n-1}t,\\ &w = -\tfrac{\sqrt{a\nu_f}}{\sqrt{\frac{n+1}{2}}x^{\frac{n-1}{2}}}\left[nx^{n-1}f(\eta,\tau) + x^{n-1}\left(\tfrac{n-1}{2}\right)\left(\eta\tfrac{\partial f(\eta,\tau)}{\partial \eta} - f(\eta,\tau)\right)\right], \end{aligned} \tag{26}$$

The final form of the transformed differential equations after inserting Eq. (26) into the unsteady Eqs. (23)–(25) are

$$\left(\frac{\mu_{hnf}/\mu_f}{\rho_{hnf}/\rho_f}\right)\frac{\partial^3 f}{\partial \eta^3} + f\frac{\partial^2 f}{\partial \eta^2} - \frac{2n}{n+1}\left(\frac{\partial f}{\partial \eta}\right)^2 - \frac{\partial^2 f}{\partial \eta \partial \tau} = 0 \tag{27}$$

$$\left(\frac{\mu_{hnf}/\mu_f}{\rho_{hnf}/\rho_f}\right)\frac{\partial^3 g}{\partial \eta^3} + f\frac{\partial^2 g}{\partial \eta^2} - \frac{2n}{n+1}\left(\frac{\partial f}{\partial \eta}\frac{\partial g}{\partial \eta}\right) - \frac{\partial^2 g}{\partial \eta \partial \tau} = 0 \tag{28}$$

$$\frac{1}{\mathrm{Pr}}\frac{k_{hnf}/k_f}{(\rho C_p)_{hnf}/(\rho C_p)_f}\frac{\partial^2 \theta}{\partial \eta^2} + f\frac{\partial \theta}{\partial \eta} - \frac{\partial \theta}{\partial \tau} = 0 \tag{29}$$

while the former condition (19) become

$$\begin{aligned} &f(0,\tau) = S,\ g(0,\tau) = 0,\ \tfrac{\partial f(0,\tau)}{\partial \eta} = \lambda,\ \tfrac{\partial g(0,\tau)}{\partial \eta} = \lambda,\ \theta(0,\tau) = 1,\\ &\tfrac{\partial f(\eta,\tau)}{\partial \eta} \to 0,\ \tfrac{\partial g(\eta,\tau)}{\partial \eta} \to 0,\ \theta(\eta,\tau) \to 0,\ \text{as } \eta \to \infty. \end{aligned} \tag{30}$$

The perturbation equations as imposed by Weidman et al. [54] is substituted into Eqs. (27)–(30) so that

$$\frac{\mu_{hnf}/\mu_f}{\rho_{hnf}/\rho_f}F''' + f_0F'' - \left(\frac{4n}{n+1}f'_0 - \gamma\right)F' + f''_0F = 0, \tag{31}$$

$$\frac{\mu_{hnf}/\mu_f}{\rho_{hnf}/\rho_f}G''' + f_0G'' - \left(\frac{2n}{n+1}f'_0 - \gamma\right)G' - \frac{2n}{n+1}F'g'_0 + Fg''_0 = 0, \tag{32}$$

$$\frac{1}{\mathrm{Pr}}\frac{k_{hnf}/k_f}{(\rho C_p)_{hnf}/(\rho C_p)_f}H'' + F\theta'_0 + f_0H' + \gamma H = 0, \tag{33}$$

with the homogeneous boundary condition

$$\begin{aligned} &F(0) = 0,\ F'(0) = 0,\ G(0) = 0,\ G'(0) = 0,\ H(0) = 0,\\ &F'(\eta) \to 0,\ G'(\eta) \to 0,\ H(\eta) \to 0,\ \text{as } \eta \to \infty. \end{aligned} \tag{34}$$

The perturbation equations (see Weidman et al. [54]) are

$$\left.\begin{aligned} f(\eta,\tau) &= f_0(\eta) + e^{-\gamma\tau}F(\eta),\\ g(\eta,\tau) &= g_0(\eta) + e^{-\gamma\tau}G(\eta),\\ \theta(\eta,\tau) &= \theta_0(\eta) + e^{-\gamma\tau}H(\eta), \end{aligned}\right\} \tag{35}$$

where $f_0(\eta) = f(\eta)$, $g_0(\eta) = g(\eta)$, $\theta_0(\eta) = \theta(\eta)$ and γ is an eigenvalue. The equations in (35) are important to test the solutions' stability where the sign value of the smallest eigenvalue γ_1 will determine the real (physical) solution. Harris et al. [55] suggested that by substituting a suitable far-field boundary condition ($F'(\infty)$,$G'(\infty)$ or $H(\infty)$) with a new condition, a nontrivial solution/eigenvalue can be gained. Hence, in the study, $F'(\infty) \to 0$ in Eq. (35) is replaced with $F''(0) = 1$ and the new condition to replace the homogeneous boundary condition is

$$F(0)=0,\ F'(0)=0,\ F''(0)=1,\ G(0)=0,\ G'(0)=0,\ H(0)=0,$$
$$G'(\eta)\to 0,\ H(\eta)\to 0,\ \text{as}\ \eta\to\infty. \tag{36}$$

The flow stability is analysed using the bvp4c solver (continuation code from the steady flow). The resulting smallest eigenvalue may determine the real (physical) solution; $\gamma_1 > 0$ indicates the real (physical) solution while negative γ_1 implies the unreal solution.

4. Results and discussion

Matlab software through the bvp4c function is utilized as the main tool for the numerical computation. Similarity differential equations as stated in Eqs. (15)–(17) together with the condition (19) are computed to observe the flow and heat transfer characteristics while the non-uniqueness of the solutions are also being the main interest of the present work. Two set of initial guesses are required to find the non-unique solutions which fulfil all the far field boundary conditions ($f'(\eta)\to 0$, $g'(\eta)\to 0$, $\theta(\eta)\to 0$). In the present work, $\eta_\infty = 15$ is used for searching the possible similarity solutions (first and second) with the disparate values of the governing parameters as highlighted in the figures and tables. For the verification of the present method, the model when $\phi_1=\phi_2=0$, $\lambda=-1$ and $n=1$ is solved and graphically presented. Fig. 2 shows that the result is in conjunction with Miklavčič and Wang [8] where dual solutions are obtainable when $S>2$, no solution when $S<2$ and distinctive solution at $S=2$.

In addition, Tables 4 and 5 elucidate the comparison values of $f''(0)$ and $-\theta'(0)$ between present correlation (following Devi and Devi [29,30]), correlation in Table 3 (following Takabi and Salehi [47] and Ghalambaz et al. [48]) and those by Waini et al. [34] when $\mathrm{Pr}=6.2$, $S=2.1$, $\lambda=-1$ and $\phi_1=0$, $\phi_2=0.2$ (Cu-water nanofluid). The comparison values are in a good agreement; hence, it shows that the present method is applicable to solve the current problem. For future reference, we also include the values of ${Re_x}^{1/2}C_{fx}$ and ${Re_x}^{-1/2}Nu_x$ when $n>1$ (nonlinear shrinking velocity) which are not considered by Waini et al. [34]. The value of ${Re_x}^{1/2}C_{fx}$ and ${Re_x}^{-1/2}Nu_x$ of first solution increase when n is added which implies that the Cu-water nanofluid with nonlinear shrinking case has greater heat transfer rate than the linear shrinking case.

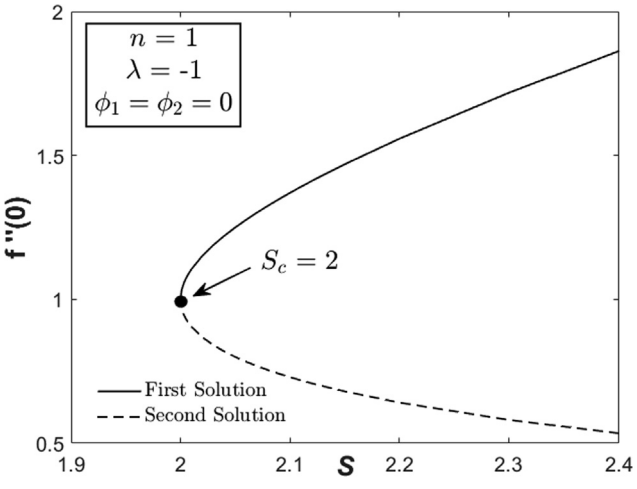

Fig. 2 $f''(0)$ against S when $n=1$.

Tables 6 and 7 present the values of ${Re_x}^{1/2}C_{fx}$ and ${Re_x}^{-1/2}Nu_x$, respectively when $S=2.5$, $\lambda=-1$, $\phi_1=0.1$, $n=1$ and various ϕ_2 using thermophysical properties of hybrid nanofluid in Table 1 (following Devi and Devi [29,30]) and Table 3 (following Takabi and Salehi [47] and Ghalambaz et al. [48]) for future reference. It is worth to point out that the values of ${Re_x}^{1/2}C_{fx}$ and ${Re_y}^{1/2}C_{fy}$ are same, hence we only provide the value of ${Re_x}^{1/2}C_{fx}$ in Table 6. Both correlations have same values of ${Re_x}^{1/2}C_{fx}$ and ${Re_x}^{-1/2}Nu_x$ when a reduced case of nanofluid is considered ($\phi_2=0$). Meanwhile, both correlations show a similar pattern where ${Re_x}^{1/2}C_{fx}$ (first and second solutions) increases and ${Re_x}^{-1/2}Nu_x$ (first and second solutions) decreases as ϕ_2 increases.

Here, the parameters are specified within the range of $0\leqslant\phi_2\leqslant 0.02$, $2<S\leqslant 2.5$ and $1\leqslant n\leqslant 3$ while the values of $\mathrm{Pr}=6.2$, $\phi_1=0.1$ and $\eta_\infty=15$ are immovable. These values are used based on the main literatures and occurrence of the non-unique solutions. The numerical solutions are presented in the tables and graphs. First solution as displayed in Figs. 3–10 is assigned to the first solution which fulfil Eq. (19). Table 8 assembles the critical (minimal/maximal) values with different n, S and ϕ_2. The critical value λ_c is the joint point of two solutions (first and second) where no unique or multiple solutions may exist when $\lambda<\lambda_c$. Boundary layer starts separating when $\lambda<\lambda_c$ and at this condition, Eqs. (15)–(17) cannot be used to observe the flow characteristics. λ_c also known as separation point and usually locates at the shrinking region ($\lambda<0$). This is one of the reasons why the authors consider shrinking flow. Based on Table 8, the separation point can be extended when ϕ_2 and S increase whereas the addition of n reduces λ_c. A boost in suction and copper nanoparticles volume fraction can delay the separation. Surprisingly, linear stretching/shrinking velocity ($n=1$) is better than the power-law velocity ($n=2,3$) in preventing the separation.

The dual solutions can be reached for both alumina-water nanofluid ($\phi_1=0.1,\phi_2=0$) and Cu-Al_2O_3/water hybrid nanofluid ($\phi_1=0.1,\phi_2=0.01,0.02$) only if the suction parameter is imposed as exhibited in Figs. 3 and 4. The values of the reduced skin friction coefficients in $x-$ and $y-$directions are same since the hybrid nanofluid flow is axisymmetric. An upsurge of the copper nanoparticles volume fraction lead to the reduction of suction's critical or minimal value where $S_c=2.09471$ ($\phi_2=0$), $S_c=2.06125$ ($\phi_2=0.01$) and $S_c=2.03172$ ($\phi_2=0.02$). The values of the reduced skin friction coefficients (first solution) increase when ϕ_2 is increased. It also evident from Fig. 3, both ${Re_x}^{1/2}C_{fx}$ and ${Re_y}^{1/2}C_{fy}$ (first solution) slightly escalate as S enhances which applicable for all values of ϕ_2. Fig. 4 reveals that the alumina-water nanofluid has higher heat transfer rate than hybrid Cu-Al_2O_3/water nanofluid when the flow is induced by the shrinking sheet ($\lambda=-1$). However, the enhancement of suction's strength can boost the heat transfer rate for both nanofluids. Suction acts as a booster for the heated fluid motion towards the sheet/plate and consequently, increase the ${Re_x}^{-1/2}Nu_x$.

Figs. 5–8 display the variations of ${Re_x}^{1/2}C_{fx}$, ${Re_y}^{1/2}C_{fy}$ and ${Re_x}^{-1/2}Nu_x$ against λ with the accretion of power exponent parameter n, suction parameter S and copper nanoparticles

Table 4 Comparison values of $f''(0)$ with Waini et al. [34] when $S = 2.1$ and $\lambda = -1$ for Cu-water nanofluid ($\phi_2 = 0.2$).

	Present (Correlation in Table 1)		Present (Correlations in Table 3)		Waini et al. [34]	
	First solution	Second solution	First solution	Second solution	First solution	Second solution
$n = 1$	2.528970	0.584729	2.528970	0.584729	2.528984	0.584729
	(4.417930)	(1.021479)	(4.417930)	(1.021479)	(–)	(–)
$n = 2$	2.407222	0.186276	2.407222	0.186276	–	–
	(5.150351)	(0.398546)	(5.150351)	(0.398546)		
$n = 3$	2.342192	0.091798	2.342192	0.091798	–	–
	(5.786453)	(0.226790)	(5.786453)	(0.226790)		

() indicates the value of $Re_x^{1/2}C_{fx}$ and $Re_y^{1/2}C_{fy}$

Table 5 Comparison values of $-\theta'(0)$ with Waini et al. [34] when $S = 2.1$ and $\lambda = -1$ for Cu-water nanofluid ($\phi_2 = 0.2$).

	Present (Correlation in Table 1)		Present (Correlation in Table 3)		Waini et al. [34]	
	First solution	Second solution	First solution	Second solution	First solution	Second solution
$n = 1$	6.822453	6.693105	6.822453	6.693105	6.822454	6.693105
	(11.910011)	(11.684207)	(11.91001)	(11.684207)	(–)	(–)
$n = 2$	6.817936	6.669567	6.817936	6.669567	–	–
	(14.577066)	(14.259847)	(14.57706)	(14.259847)		
$n = 3$	6.815464	6.666046	6.815464	6.666046	–	–
	(16.826043)	(16.457159)	(16.82604)	(16.457159)		

() indicates the value of $Re_x^{-1/2}Nu_x$.

Table 6 Comparison values of $Re_x^{1/2}C_{fx}$ between correlations of hybrid nanofluids in Table 1 and Table 3 when $S = 2.5$, $\lambda = -1$, $\phi_1 = 0.1$, $n = 1$ and various ϕ_2.

	Present (Correlation in Table 1)		Present (Correlation in Table 3)	
	First solution	Second solution	First solution	Second solution
$\phi_2 = 0$	2.594178	0.645222	2.594178	0.645222
$\phi_2 = 0.01$	2.776053	0.653350	2.781516	0.655350
$\phi_2 = 0.02$	2.956487	0.662716	2.967257	0.666894
$\phi_2 = 0.03$	3.135633	0.673176	3.151544	0.679725

Table 7 Comparison values of $Re_x^{-1/2}Nu_x$ between correlations of hybrid nanofluids in Table 1 and Table 3 when $S = 2.5$, $\lambda = -1$, $\phi_1 = 0.1$, $n = 1$ and various ϕ_2.

	Present (Correlation in Table 1)		Present (Correlation in Table 3)	
	First solution	Second solution	First solution	Second solution
$\phi_2 = 0$	14.609110	14.537865	14.609110	14.537865
$\phi_2 = 0.01$	14.577530	14.497776	14.572071	14.491916
$\phi_2 = 0.02$	14.545834	14.457310	14.536181	14.447358
$\phi_2 = 0.03$	14.514012	14.416449	14.500420	14.402851

concentration ϕ_2. The values of $Re_x^{1/2}C_{fx}$ and $Re_y^{1/2}C_{fy}$ of first solution for Cu-Al_2O_3/water hybrid nanofluid enhance with the increment of n and S for the shrinking case ($\lambda < 0$) as presented in Figs. 5 and 6. However, contrary results are obtained for the stretching case ($\lambda > 0$). Besides, $Re_x^{1/2}C_{fx}$ and $Re_y^{1/2}C_{fy}$ of second solution decrease with the increment of n and S for both stretching and shrinking cases. It is noted that n is a power exponent parameter for the velocity distribution; $n = 1$ denotes the linear form of stretching/shrinking velocity while $n > 1$ indicates the nonlinear or power-law velocity. As manifested in Fig. 7, the nonlinear form of plate motion can develop the heat transfer rate for both cases. It seems that the heat transfer rate for stretching case are always greater than shrinking case for all selected values of n. Fig. 8 reveals that the value of $Re_x^{-1/2}Nu_x$ deteriorates with the increment of copper nanoparticles volume fraction for both stretching and shrinking cases. Like Fig. 7, the heat transfer rate are greater for stretching case.

Figs. 9 and 10 demonstrate the velocities in both $x-$,$y-$directions and temperature profiles when $\lambda = 1$ (stretching), $\lambda = -1$ (shrinking), $n = 1$ (linear plate motion) and $n = 2$ (nonlinear plate motion). Fig. 9 reveals that the first solution

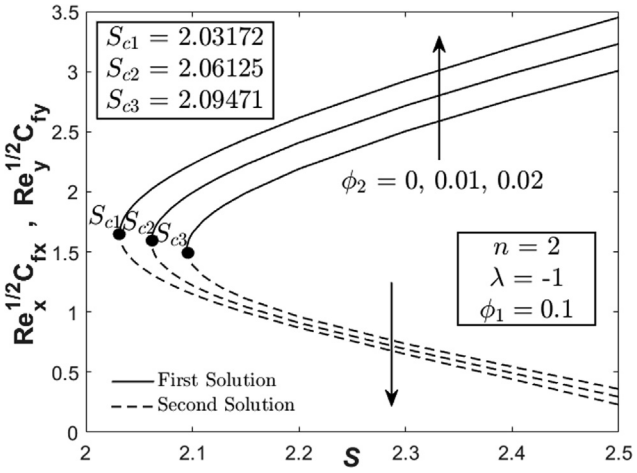

Fig. 3 $Re_x^{1/2}C_{fx}$ and $Re_y^{1/2}C_{fy}$ towards S for various ϕ_2.

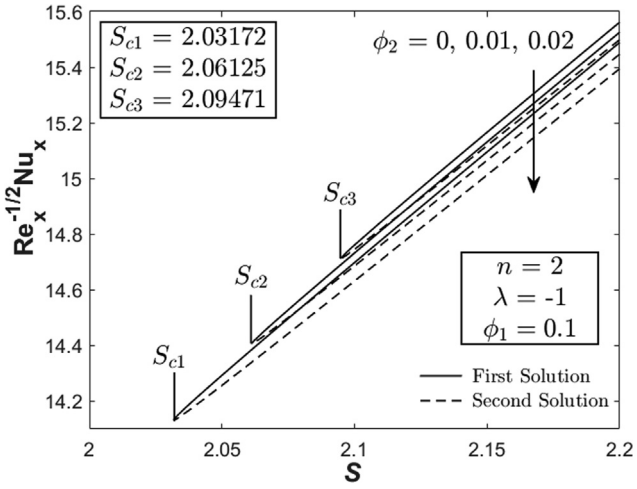

Fig. 4 $Re_x^{-1/2}Nu_x$ towards S for various ϕ_2.

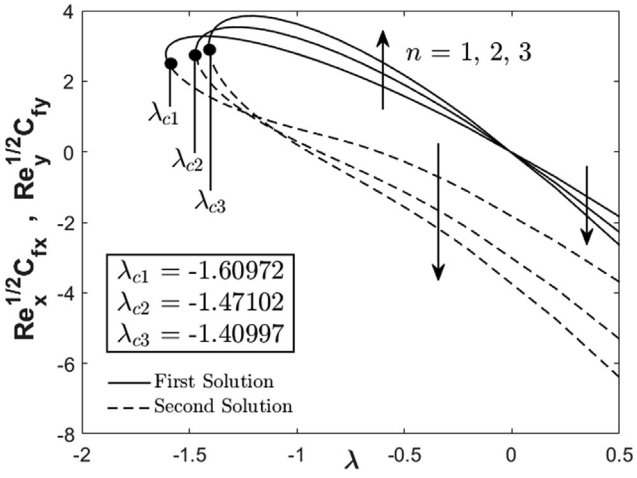

Fig. 5 $Re_x^{1/2}C_{fx}$ and $Re_y^{1/2}C_{fy}$ towards λ for various n when $S = 2.5$ and $\phi_2 = 0.01$.

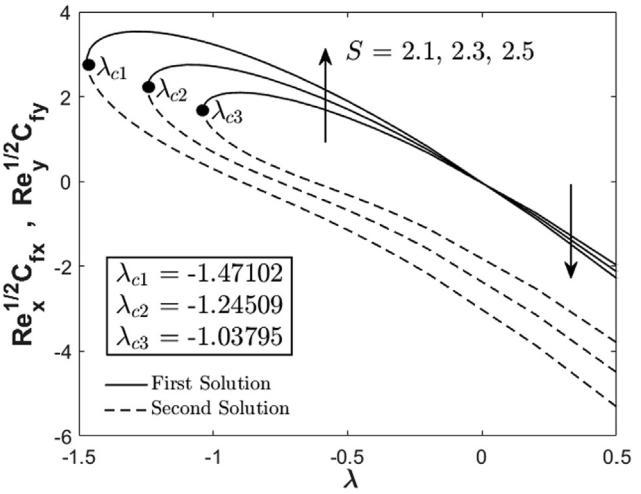

Fig. 6 $Re_x^{1/2}C_{fx}$ and $Re_y^{1/2}C_{fy}$ towards λ for various S when $n = 2$ and $\phi_2 = 0.01$.

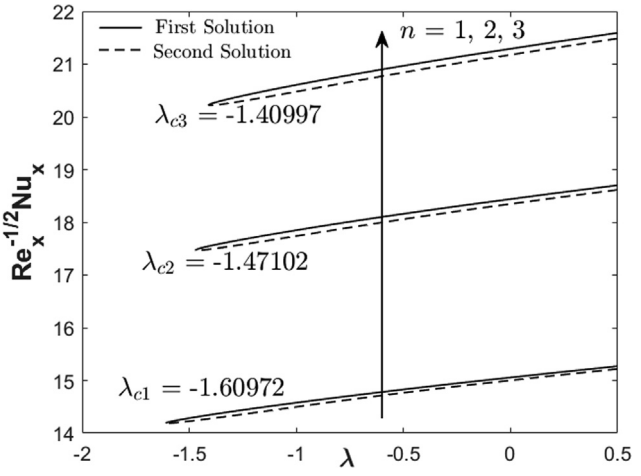

Fig. 7 $Re_x^{-1/2}Nu_x$ towards λ for various n when $S = 2.5$ and $\phi_2 = 0.01$.

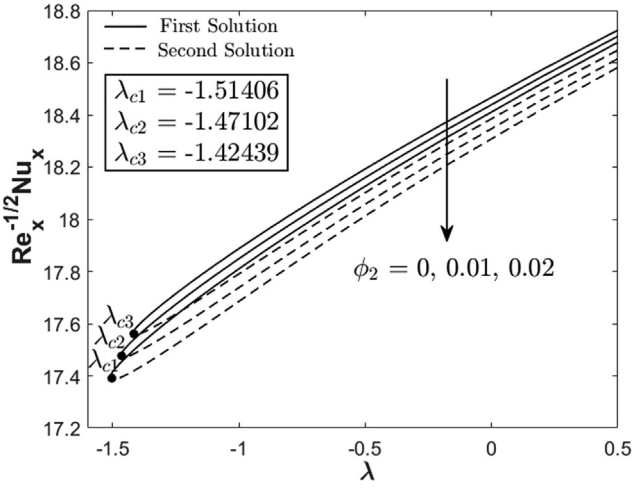

Fig. 8 $Re_x^{-1/2}Nu_x$ towards λ for various ϕ_2 when $S = 2.5$ and $n = 2$.

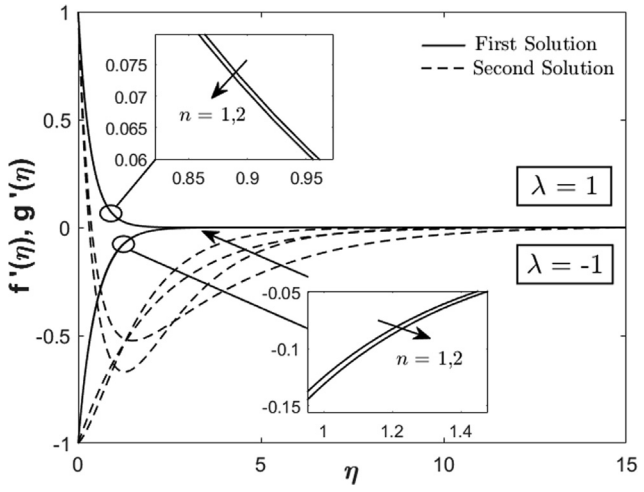

Fig. 9 $f'(\eta)$ and $g'(\eta)$ for stretching and shrinking cases when $\phi_2 = 0.01$ and $S = 2.5$.

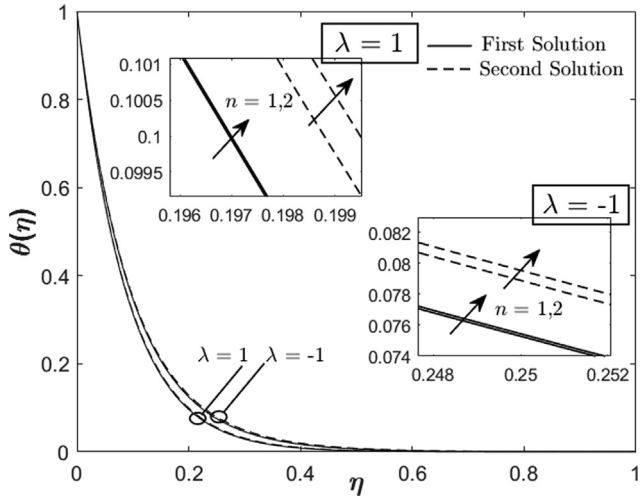

Fig. 10 $\theta(\eta)$ for stretching and shrinking cases when $\phi_2 = 0.01$ and $S = 2.5$.

Table 8 Critical values λ_c for assorted values of n, S and ϕ_2.

S	n	ϕ_2	λ_c
2.5	2	0	−1.42439
2.5	2	0.01	−1.47102
2.5	2	0.02	−1.51406
2.3	2	0.01	−1.24509
2.1	2	0.01	−1.03795
2.5	1	0.01	−1.60972
2.5	3	0.01	−1.40997

of both velocities is symmetric when $\lambda = 1$ and $\lambda = -1$. However, the second solution has different characteristics and seemed to be unstable. The temperature of hybrid nanofluid intensifies as n increases for both stretching and shrinking cases as displayed in Fig. 10. Fluid temperature is seemed to be higher for the shrinking case than the stretching case. Fig. 11 expounds the smallest eigenvalue γ_1 of first and second

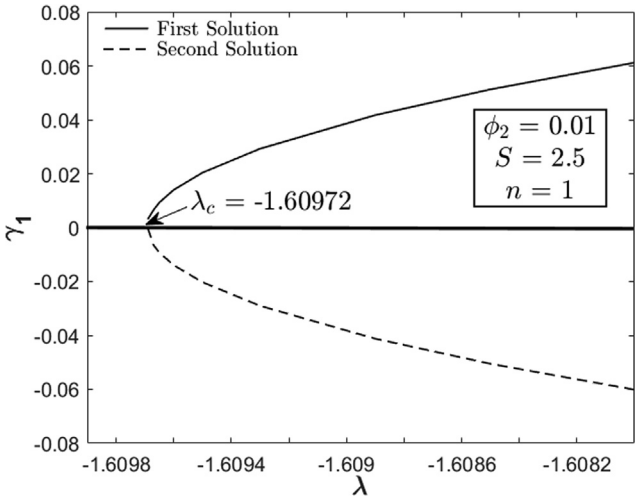

Fig. 11 γ_1 of first and second solutions against λ when $\phi_2 = 0.01$, $S = 2.5$ and $n = 1$.

solutions towards $\lambda_c = -1.60972$. This result is achieved by solving Eqs. (31)–(33) and (36) through the efficient bvp4c function. $\gamma_1 > 0$ implies that the first solution is undoubtedly stable whereas the second solution is unreal. In addition, both (first and second) γ_1 approach to 0 as $\lambda \to \lambda_c$ which complies with Merkin [53]. This signifies that the first and second solutions bifurcate at the critical value.

5. Conclusions

The present problem emphasizes the three-dimensional flow and heat transfer of Cu-Al_2O_3/water hybrid nanofluid towards a power law (nonlinear) permeable stretching/shrinking sheet with orthogonal surface shear. The conclusions are as follows:

- The flow due to the shrinking sheet is possible with two solutions if the suction parameter $S > 2$ is applied. The stretching flow up to $\lambda = 0.5$ also has dual solutions.
- The separation point can be extended when ϕ_2 and S increase whereas the addition of n accelerates the boundary layer separation. The linear plate velocity is better in holding the separation process than the nonlinear velocity for this problem.
- Alumina-water nanofluid has higher heat transfer rate than hybrid Cu-Al_2O_3/water nanofluid when the flow is induced by the nonlinear shrinking sheet.
- The enlargement of S and n can increase the heat transfer rate whereas the opposite result is obtained for the ϕ_2.
- The stability analysis affirms that the first (upper branch) solution is stable whereas the second (lower branch) solution is unstable.
- The temperature profile increases with the enhancement of nonlinear parameter n for both stretching and shrinking cases. However, the temperature profile of stretching flow is lower than the shrinking flow.

Declaration of Competing Interest

There are no conflict of interest between the authors.

Acknowledgements

The financial support through the Fundamental Research Grant Scheme (FRGS)–5540309 from Ministry of Education (Malaysia) and JURNAL/2019/FTKMP/Q00048 from Universiti Teknikal Malaysia Melaka are appreciatively acknowledged including the support from Universiti Putra Malaysia. The authors wish also to express their thanks to the very competent Reviewers for the very good comments and suggestions.

References

[1] L.J. Crane, Flow past a stretching plate, Zeitschrift für angewandte Mathematik und Physik ZAMP 21 (4) (1970) 645–647.
[2] W.H. Banks, Similarity solutions of the boundary-layer equations for a stretching wall, J. Mécanique théorique et appliquée 2 (1983) 375–392.
[3] P. Weidman, Flows induced by power-law stretching surface motion modulated by transverse or orthogonal surface shear, Comptes Rendus Mécanique 345 (2) (2017) 169–176.
[4] P.D. Weidman, Flows induced by flat surfaces sheared in their own plane, Fluid Dynam. Res. 45 (1) (2013) 015506.
[5] P.D. Weidman, The motion induced by the orthogonal stretching and shearing of a membrane beneath a quiescent fluid, Acta Mech. 226 (10) (2015) 3307–3316.
[6] P.D. Weidman, S. Mansur, A. Ishak, Biorthogonal stretching and shearing of an impermeable surface in a uniformly rotating fluid system, Meccanica 52 (7) (2017) 1515–1525.
[7] S. Goldstein, On backward boundary layers and flow in converging passages, J. Fluid Mech. 21 (1) (1965) 33–45.
[8] M. Miklavčič, C. Wang, Viscous flow due to a shrinking sheet, Q. Appl. Math. 64 (2) (2006) 283–290.
[9] T. Fang, Boundary layer flow over a shrinking sheet with power-law velocity, Int. J. Heat Mass Transf. 51 (25–26) (2008) 5838–5843.
[10] S. Suresh, K.P. Venkitaraj, P. Selvakumar, M. Chandrasekar, Synthesis of Al2O3–Cu/water hybrid nanofluids using two step method and its thermo physical properties, Colloid Surf. A-Physicochem. Eng. Asp. 388 (1–3) (2011) 41–48.
[11] D. Mansoury, F.I. Doshmanziari, S. Rezaie, M.M. Rashidi, Effect of Al2O3/water nanofluid on performance of parallel flow heat exchangers, J. Therm. Anal. Calorim. 135 (1) (2019) 625–643.
[12] Y. Ma, R. Mohebbi, M.M. Rashidi, O. Manca, Z. Yang, Numerical investigation of MHD effects on nanofluid heat transfer in a baffled U-shaped enclosure using lattice Boltzmann method, J. Therm. Anal. Calorim. 135 (6) (2019) 3197–3213.
[13] S. Jana, A. Salehi-Khojin, W.H. Zhong, Enhancement of fluid thermal conductivity by the addition of single and hybrid nano-additives, Thermochim. Acta 462 (1–2) (2007) 45–55.
[14] J. Sarkar, P. Ghosh, A. Adil, A review on hybrid nanofluids: recent research, development and applications, Renew. Sust. Energ. Rev. 43 (2015) 164–177.
[15] N.A. Sidik, I.M. Adamu, M.M. Jamil, G.H. Kefayati, R. Mamat, G. Najafi, Recent progress on hybrid nanofluids in heat transfer applications: a comprehensive review, Int. Comm. Heat Mass Transf. 78 (2016) 68–79.
[16] S. Akilu, K.V. Sharma, A.T. Baheta, R. Mamat, A review of thermophysical properties of water based composite nanofluids, Renew. Sust. Energ. Rev. 66 (2016) 654–678.
[17] J.R. Babu, K.K. Kumar, S.S. Rao, State-of-art review on hybrid nanofluids, Renew. Sust. Energ. Rev. 77 (2017) 551–565.
[18] L.S. Sundar, K.V. Sharma, M.K. Singh, A.C. Sousa, Hybrid nanofluids preparation, thermal properties, heat transfer and friction factor–a review, Renew. Sust. Energ. Rev. 68 (2017) 185–198.
[19] K.Y. Leong, K.K. Ahmad, H.C. Ong, M.J. Ghazali, A. Baharum, Synthesis and thermal conductivity characteristic of hybrid nanofluids–a review, Renew. Sust. Energ. Rev. 75 (2017) 868–878.
[20] G. Huminic, A. Huminic, Hybrid nanofluids for heat transfer applications–a state-of-the-art review, Int. J. Heat Mass Transf. 125 (2018) 82–103.
[21] M.U. Sajid, H.M. Ali, Thermal conductivity of hybrid nanofluids: a critical review, Int. J. Heat Mass Transf. 126 (2018) 211–234.
[22] M. Ghalambaz, S.A. Mehryan, A. Hajjar, A. Veisimoradi, Unsteady natural convection flow of a suspension comprising Nano-Encapsulated Phase Change Materials (NEPCMs) in a porous medium, Adv. Powder Tech. (2019), https://doi.org/10.1016/j.apt.2019.12.010.
[23] M. Ghalambaz, A.J. Chamkha, D. Wen, Natural convective flow and heat transfer of nano-encapsulated phase change materials (NEPCMs) in a cavity, Int. J. Heat Mass Transf. 138 (2019) 738–749.
[24] M. Ghalambaz, T. Groşan, I. Pop, Mixed convection boundary layer flow and heat transfer over a vertical plate embedded in a porous medium filled with a suspension of nano-encapsulated phase change materials, J. Mol. Liq. 293 (2019) 111432.
[25] A. Hajjar, S.A. Mehryan, M. Ghalambaz, Time periodic natural convection heat transfer in a nano-encapsulated phase-change suspension, Int. J. Mech. Sci. 166 (2020) 105243.
[26] A.J. Chamkha, I.V. Miroshnichenko, M.A. Sheremet, Numerical analysis of unsteady conjugate natural convection of hybrid water-based nanofluid in a semicircular cavity, J. Therm. Sci. Eng. Appl. 9 (4) (2017) 041004.
[27] M. Ghalambaz, M.A. Sheremet, S.A. Mehryan, F.M. Kashkooli, I. Pop, Local thermal non-equilibrium analysis of conjugate free convection within a porous enclosure occupied with Ag–MgO hybrid nanofluid, J. Therm. Anal. Calorim. 135 (2) (2019) 1381–1398.
[28] M.A. Sheremet, D.S. Cimpean, I. Pop, Thermogravitational convection of hybrid nanofluid in a porous chamber with a central heat-conducting body, Symmetry 12 (4) (2020) 593.
[29] S.A. Devi, S.S. Devi, Numerical investigation of hydromagnetic hybrid Cu–Al2O3/water nanofluid flow over a permeable stretching sheet with suction, Int. J. Nonlin. Sci. Numer. Simul. 17 (5) (2016) 249–257.
[30] S.S.U. Devi, S.P.A. Devi, Heat transfer enhancement of Cu–Al2O3/water hybrid nanofluid flow over a stretching sheet, J. Nigerian Math. Soc. 36 (2017) 419–433.
[31] R.K. Tiwari, M.K. Das, Heat transfer augmentation in a two-sided lid-driven differentially heated square cavity utilizing nanofluids, Int. J. Heat Mass Transf. 50 (9–10) (2007) 2002–2018.
[32] E. Abu-Nada, Application of nanofluids for heat transfer enhancement of separated flows encountered in a backward facing step, Int. J. Heat Fluid Flow 29 (1) (2008) 242–249.
[33] I. Waini, A. Ishak, I. Pop, Hybrid nanofluid flow and heat transfer over a nonlinear permeable stretching/shrinking surface, Int. J. Numer. Methods Heat Fluid Flow 29 (9) (2019) 3110–3127.
[34] I. Waini, A. Ishak, I. Pop, Unsteady flow and heat transfer past a stretching/shrinking sheet in a hybrid nanofluid, Int. J. Heat Mass Transf. 136 (2019) 288–297.
[35] I. Waini, A. Ishak, I. Pop, Transpiration effects on hybrid nanofluid flow and heat transfer over a stretching/shrinking sheet with uniform shear flow, Alex. Eng. J. 59 (1) (2020) 91–99.
[36] N.S. Khashi'ie, N.M. Arifin, R. Nazar, E.H. Hafidzuddin, N. Wahi, I. Pop, Magnetohydrodynamics (MHD) axisymmetric flow and heat transfer of a hybrid nanofluid past a radially

permeable stretching/shrinking sheet with joule heating, Chin. J. Phys. 64 (2020) 251–263.
[37] L.A. Lund, Z. Omar, I. Khan, A.H. Seikh, E.S. Sherif, K.S. Nisar, Stability analysis and multiple solution of Cu–Al_2O_3/H_2O nanofluid contains hybrid nanomaterials over a shrinking surface in the presence of viscous dissipation, J. Mater. Res. Technol. 9 (1) (2019) 421–432.
[38] S. Dinarvand, M.N. Rostami, I. Pop, A novel hybridity model for TiO 2-CuO/water hybrid nanofluid flow over a static/moving wedge or corner, Sci. Rep. 9 (1) (2019) 1.
[39] S. Dinarvand, M.N. Rostami, R. Dinarvand, I. Pop, Improvement of drug delivery micro-circulatory system with a novel pattern of CuO-Cu/blood hybrid nanofluid flow towards a porous stretching sheet, Int. J. Numer. Methods Heat Fluid Flow 29 (11) (2019) 4408–4429.
[40] S. Dinarvand, M. Yousefi, A. Chamkha, Numerical simulation of unsteady flow toward a stretching/shrinking sheet in porous medium filled with a hybrid nanofluid, J. Appl. Comp. Mech. (2019), https://doi.org/10.22055/JACM.2019.29407.1595.
[41] E.H. Aly, I. Pop, MHD flow and heat transfer over a permeable stretching/shrinking sheet in a hybrid nanofluid with a convective boundary condition, Int. J. Numer. Methods Heat Fluid Flow 29 (9) (2019) 3012–3038.
[42] U. Farooq, M.I. Afridi, M. Qasim, D.C. Lu, Transpiration and viscous dissipation effects on entropy generation in hybrid nanofluid flow over a nonlinear radially stretching disk, Entropy 20 (9) (2018) 668.
[43] N.S. Khashi'ie, N.M. Arifin, I. Pop, R. Nazar, E.H. Hafidzuddin, N. Wahi, Non-axisymmetric Homann stagnation point flow and heat transfer past a stretching/shrinking sheet using hybrid nanofluid, Int. J. Numer. Methods Heat Fluid Flow 2020. https://doi.org/10.1108/HFF-11-2019-0824.
[44] N.S. Khashi'ie, N.M. Arifin, I. Pop, R. Nazar, E.H. Hafidzuddin, N. Wahi, Thermal Marangoni Flow Past a Permeable Stretching/Shrinking Sheet in a Hybrid Cu-Al2O3/Water Nanofluid. Sains Malaysiana 49(1) (2020) 211–222.
[45] K. Khanafer, K. Vafai, M. Lightstone, Buoyancy-driven heat transfer enhancement in a two-dimensional enclosure utilizing nanofluids, Int. J. Heat Mass Transf. 46 (19) (2003) 3639–3653.
[46] H.F. Oztop, E. Abu-Nada, Numerical study of natural convection in partially heated rectangular enclosures filled with nanofluids, Int. J. Heat Fluid Flow 29 (5) (2008) 1326–1336.
[47] B. Takabi, S. Salehi, Augmentation of the heat transfer performance of a sinusoidal corrugated enclosure by employing hybrid nanofluid, Adv. Mech. Eng. 6 (2014) 147059.
[48] M. Ghalambaz, N.C. Roşca, A.V. Roşca, I. Pop, Mixed convection and stability analysis of stagnation-point boundary layer flow and heat transfer of hybrid nanofluids over a vertical plate, Int. J. Numer. Methods Heat Fluid Flow (2019), https://doi.org/10.1108/HFF-08-2019-0661.
[49] T. Tayebi, A.J. Chamkha, Entropy generation analysis during MHD natural convection flow of hybrid nanofluid in a square cavity containing a corrugated conducting block, Int. J. Numer. Methods Heat Fluid Flow 30 (3) (2019) 1115–1136.
[50] P.D. Weidman, A.M. Davis, D.G. Kubitschek, Crocco variable formulation for uniform shear flow over a stretching surface with transpiration: multiple solutions and stability, Zeitschrift für angewandte Mathematik und Physik 59 (2) (2008) 313–332.
[51] N.S. Khashi'ie, N. Md Arifin, R. Nazar, E.H. Hafidzuddin, N. Wahi, I. Pop, A stability analysis for magnetohydrodynamics stagnation point flow with zero nanoparticles flux condition and anisotropic slip, Energies 2(7) (2019) 1268.
[52] N.S. Khashi'ie, N.M. Arifin, E.H. Hafidzuddin, N. Wahi, Dual stratified nanofluid flow past a permeable shrinking/stretching sheet using a non-Fourier energy model. Appl. Sci. 9(10) (2019) 2124.
[53] J.H. Merkin, On dual solutions occurring in mixed convection in a porous medium, J. Eng. Math. 20 (2) (1986) 171–179.
[54] P.D. Weidman, D.G. Kubitschek, A.M. Davis, The effect of transpiration on self-similar boundary layer flow over moving surfaces, Int. J. Eng. Sci. 44 (11–12) (2006) 730–737.
[55] S.D. Harris, D.B. Ingham, I. Pop, Mixed convection boundary-layer flow near the stagnation point on a vertical surface in a porous medium: Brinkman model with slip, Transp. Porous Media 77 (2) (2009) 267–285.